

Area rule for circulation and minimal surfaces in three-dimensional turbulence

Kartik P. Iyer,¹ Sachin S. Bharadwaj,¹ and Katepalli R. Sreenivasan^{1,2,3,*}

¹*Tandon School of Engineering, New York University, New York, NY, 11201, USA*

²*Department of Physics and the Courant Institute of Mathematical Sciences,*

New York University, New York, NY 11201, USA

³*New York University, Abu Dhabi, 129188, UAE*

An important idea underlying a plausible dynamical theory of circulation in 3D turbulence is the so-called Area Rule, according to which the probability density function (PDF) of the circulation around closed loops depends only on the minimal area of the loop. Using data from direct numerical simulations on an 8192^3 grid, we show that the tails of the PDF, characterizing large circulation amplitudes, satisfy the Area Rule. The tails of the PDFs for the minimal area of non-planar loops differ from those of planar loops circumscribing the same area, but the two agree when suitably normalized. A Gaussian Random Field with the same two-point correlation as the DNS data replicates the behavior of low-order moments of circulation but not the large amplitude universality. This work highlights the hitherto unknown connection between minimal surfaces and turbulence.

Universal features of turbulence have been explored most often in terms of the moments of velocity differences over a chosen separation distance, because they play dynamical roles in the interscale energy transfer [1] and in the characterization of the transition to turbulence [2, 3]. These so-called structure functions have been shown [4, 5] to be multifractal (i.e., moments of each order are governed by independent exponents). Multifractality has turned out to be difficult to understand analytically, and the problem is compounded because high-order structure functions for different velocity components seem to scale differently [6, 7]. It is thus reasonable to consider alternatives, one of which is the circulation around closed loops, proposed by Migdal [8]–[12]; its recent exploration in [13] has indeed shown some attractive simplicity. An underlying theme of the circulation studies is the so-called Area Rule, according to which the probability density function (PDF) of circulation around closed loops depends only on the area of the loop, not its shape (see [13–17]). This Letter explores the Area Rule for both planar and non-planar loops, and highlights the role in turbulence dynamics of minimal surfaces, which have been used extensively to model diverse phenomena such as soap films, black holes and protein folding [18–20].

The circulation around closed loop C is defined as

$$\Gamma(C) = \oint_C \mathbf{u} \cdot d\mathbf{l} = \iint_A \omega \cdot d\mathbf{A} , \quad (1)$$

where \mathbf{u} is the velocity, ω (its curl) is the vorticity and A is any area spanning C . The second equality in (1) is the Stokes' theorem. We examine the Area Rule using direct numerical simulations (DNS) of the 3D incompressible Navier-Stokes equations. The turbulence is maintained stationary by energy input at the largest scales. Details of the DNS and resulting velocity field statistics are given in [7, 21] and references therein, and will not be repeated here; only a few details are given in Table I. The inertial range for the velocity circulation is approximately

	N^3	L/η	R_λ	$u'L$	$\langle \omega^4 \rangle / \langle \omega^2 \rangle^2$
DNS	8192^3	2276	1300	1.8	22.34
GRF	8192^3	2204	–	1.7	3.00

TABLE I. A few characteristics of the DNS and GRF data in a 3D periodic cube with side $L_0 = 2\pi$ (in length units): N^3 is the grid resolution, L/η is the available scale range; for the DNS data, $L \approx 0.2L_0$ is the integral scale and $\eta \equiv (\nu^3/\langle \epsilon \rangle)^{1/4}$ is the Kolmogorov scale; here, ν is the kinematic viscosity, $\langle \epsilon \rangle$ the mean dissipation rate; R_λ is the microscale Reynolds number based on the root-mean-square velocity u' and the Taylor microscale λ , where $\lambda^2 = 15\nu u'^2/\langle \epsilon \rangle$; $u'L$ is the “large-scale circulation” to be used for various normalization purposes; $\langle \omega^4 \rangle / \langle \omega^2 \rangle^2$ is the vorticity flatness for the DNS data and the analogous quantity for the GRF. $\langle \cdot \rangle$ denotes a volume average over L_0^3 .

$r/\eta \in [50, 400]$ [13, 21], where η is the Kolmogorov scale. L/η is roughly the available scale range. We have also constructed a synthetic, divergence-free Gaussian Random Field (GRF) with the same two-point velocity correlation and the available scale range as the DNS data, with the goal of distinguishing kinematic effects from those of the Navier-Stokes dynamics [22]. Table I also gives some basic parameters of this GRF (we use L/η only in the sense of an analogue). The vorticity flatness (averaged over the three Cartesian directions) for the DNS is significantly larger than the GRF value of 3, because of the intermittency in the DNS field.

We first examine the Area Rule for rectangles in a plane. Figure 1 shows the probability density function (PDF) of circulation around rectangular loops of fixed area A but varying aspect ratios. The PDFs collapse for all rectangles as long as both their sides are contained within the inertial range. The collapsed PDFs are slightly skewed; e.g., the skewness factor is 0.02 and the hyper-skewness is about 0.5. We had therefore fitted earlier [13] the two sides of the PDF by stretched exponentials with slightly different stretch factors. The asymmetry is caused mostly from the core of the distribution;

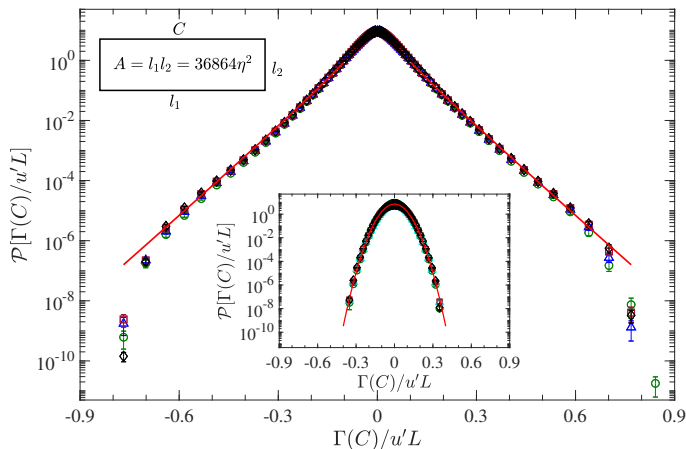


FIG. 1. PDF of circulation around a loop C with sides (l_1, l_2) and fixed planar area (shown in top left). Symbols correspond to inertial range dimensions $(l_1/\eta, l_2/\eta)$: (128, 288) (\circ), (144, 256) (\triangle), (160, 230.4) (\square), and (192, 192) (\diamond). Error bars indicate 95% confidence intervals from the student- t distribution. Solid line is the PDF fit $\alpha \exp(-bx)/\sqrt{x}$ in $x \in [0.1, 0.7]$ with $x \equiv |\Gamma(C)|/u'L$, $\alpha = 2.49$ and $b = 21.74$. The last two data points corresponding to $< (2 \times 10^{-7})\%$ samples are neglected in the fit. Inset shows corresponding PDFs for GRF with the solid line denoting the Gaussian fit $\alpha_g \exp(-b_g x^2)$ with $\alpha_g = 7.0$ and $b_g = 148.7$.

for example, the odd moments decrease with increasing order: $\langle \Gamma(C)^m \rangle / (u'L)^m$ for $m = 3, 5, 7$ and 9 are $2.6 \times 10^{-6}, 2.3 \times 10^{-7}, 2.8 \times 10^{-8}$ and 4×10^{-9} , respectively. The last two data points in Fig. 1 correspond to 1000 samples or fewer, corresponding to $< (2 \times 10^{-7})\%$ of the total number. Neglecting those points, it seems that the inertial range collapse for large $|\Gamma(C)|$ can be fitted quite well by $\alpha \exp(-b|\Gamma(C)|)/\sqrt{|\Gamma(C)|}$ [12], as shown in Fig. 1, without the need for considering the two sides of the PDFs separately. The PDF of GRF, being Gaussian by definition, possesses very few high amplitude events, as the inset shows.

While the PDFs in Fig. 1 appear to collapse, it is hard to rule out the existence of small systematic differences because of how strongly the probability axis has been squeezed. If the collapse is strictly true, the circulation moments should be independent of the loop perimeter for a fixed area. Figure 2 shows the ratio Q of the moment $\langle \Gamma(C)^m \rangle^{1/m}$ for a loop C to that for a square loop of the same area, for various orders $m = 2, 4, 6, 8, 10$ and 12 , plotted against $P = 2(l_1 + l_2)/\sqrt{A}$, where P is proportional to the arithmetic mean to the geometric mean of the sides (l_1, l_2) , bounded below by 4 for a square loop, increasing as the aspect ratio increases. If the Area Rule is exact, Q should fall on a horizontal line at unity. For $m = 2$ this ratio shows a mild but systematic decrease for inertial loops (marked by filled symbols), increasingly departing from unity as P increases. With increasing m , Q decreases further from unity but, for any chosen P ,

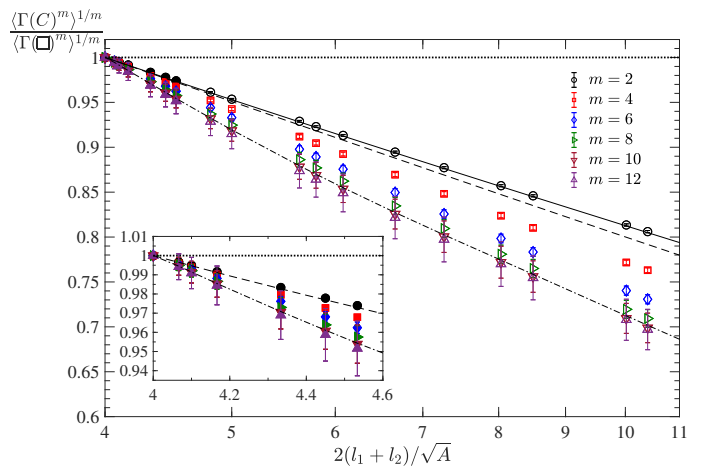


FIG. 2. The ratio Q of $\langle \Gamma(C)^m \rangle^{1/m}$ around C (see inset of Fig. 1) to that around a square loop $\langle \Gamma(\square)^m \rangle^{1/m}$ with same area plotted against normalized perimeter $P = 2(l_1 + l_2)/\sqrt{A}$ on log-linear scales. The inertial range extends between 4 and 4.6 on the P axis and is expanded in the inset in linear coordinates. Filled symbols correspond to rectangles with both sides within the inertial range while open symbols denote its complement. The dashed line is the estimate for $m = 2$ (see Eq. 2). The continuous line is the result for the GRF, and is the same for all m . For increasing moment orders m , Q departs increasingly from unity initially but saturate beyond $m \approx 8$. The dash-dot line given by $Q \approx 1.427 - 0.308 \ln P$ is an empirical fit to the asymptotic behavior.

saturates for $m \geq 8$, say. The saturation at higher orders roughly holds even for loops outside the inertial range where the ratio Q differs substantially from unity.

We will now discuss the various lines drawn in Fig. 2. First, the continuous line is for the GRF and is the same for all m . Thus, while GRF is a decent approximation to the data for $m = 2$, it is not so for high moments. For the specific case of $m = 2$, we can do better than GRF by starting with the relation [9, 10],

$$\langle \Gamma(C)^2 \rangle = \oint_C dr_i \oint_C dr'_j \langle u_i(r) u_j(r') \rangle, \quad (2)$$

if we substitute for inertial separations $\eta \ll |r - r'| \ll L$, $\langle u_i(r) u_j(r') \rangle - \delta_{ij} u^2 \propto \delta_{ij} |r - r'|^{\zeta_2}$, where ζ_2 is the scaling exponent for the second-order velocity structure function. Thus while the second-order inertial range circulation exponent is solely determined by ζ_2 , the prefactor depends on the shape of the loop, yielding a perimeter dependence of $\langle \Gamma(C)^2 \rangle$. Indeed, this second-order inertial-range estimate, calculated using $\zeta_2 = 0.72$ from [7], changes with changing aspect ratio and compares well with a direct calculation using Eq. 1. This result is shown by the dashed line in Fig. 2. The inference is that the inertial range power-law scaling of circulation moments of low orders depend on the shape of the loop, but this shape dependence decreases with increasing moment order, ultimately saturating for m beyond about 8. The

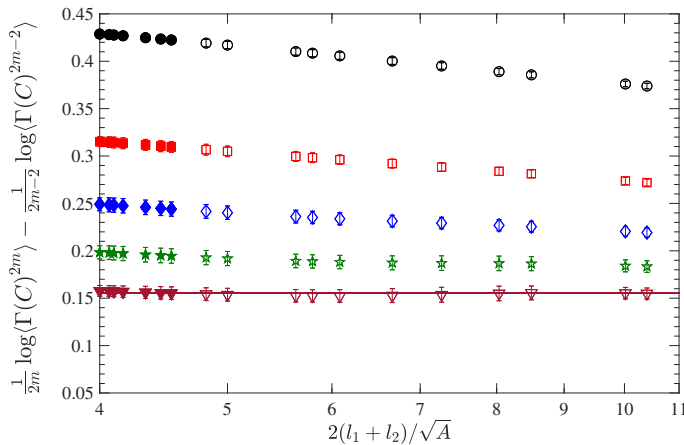


FIG. 3. Logarithm of the ratio of normalized circulation moments versus the normalized perimeter for contours with fixed A (see Fig. 1) for $m = 4, 6, 8, 10$ and 12 increasing from top to bottom. Filled symbols correspond to contours with both sides in the inertial range while open symbols correspond to contours with at least one side outside this range. Horizontal line at $m = 12$ corresponds to the high-order estimate (see Eq. 4 and the text).

saturation line for higher order moments can be fitted empirically by $Q \approx 1.427 - 0.308 \ln P$ (dash-dot line). This is not a huge variation within the inertial range here.

The fact that Q saturates for any given value of P for large enough m suggests that some scale invariance has been reached by the tails of the PDF. To explore this suggestion further, we consider the ratio of successive even-order moments as a function of the loop perimeter for various rectangles circumscribing fixed area. The logarithm of this ratio is plotted in Fig. 3 against the normalized perimeter P for different loops. The lower-order ratios show a clear perimeter dependency for inertial loops (shown by filled symbols) while the higher order ratios become perimeter independent. In contrast, without showing the result explicitly, we state that GRF shows perimeter independence (on this plot) for all values of m (approximately at values of 0.27, 0.18, 0.13, 0.10 and 0.085 for $m = 4, 6, 8, 10$ and 12 , respectively). The perimeter invariance for higher m appears to extend to loops with edge lengths well outside the inertial range.

Since higher order moments largely reside in the tails of $\mathcal{P}(\Gamma(C))$, which can be fitted quite well by the modified exponential (see Fig. 1), $\langle \Gamma(C)^m \rangle$ for large even-order m can be approximated (assuming a symmetric distribution) by

$$\langle \Gamma(C)^m \rangle \approx 2\alpha \int_0^\infty \Gamma^{m-\frac{1}{2}} e^{-b\Gamma} d\Gamma = \frac{2\alpha}{b^{m+\frac{1}{2}}} \Gamma(m+\frac{1}{2}), \quad (3)$$

where $\Gamma(z)$ is the Gamma function of z . For large m and

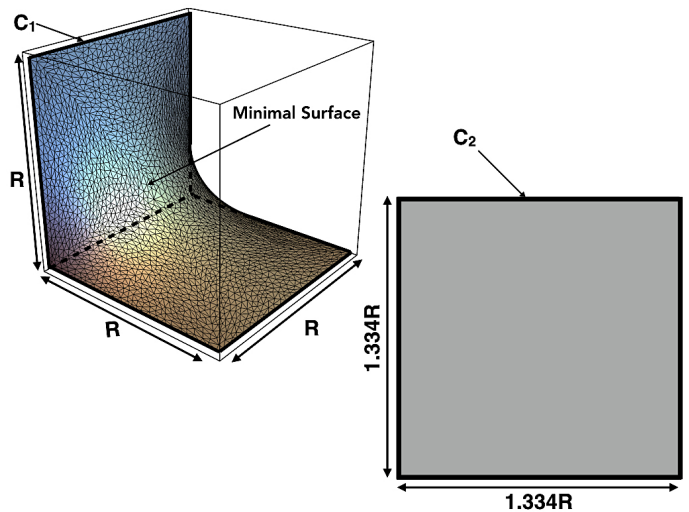


FIG. 4. Contour C_1 is a non-planar contour with side R and minimal area $A_{C_1} = 1.78R^2$. Contour C_2 is a square with the same planar area $A_{C_2} = 1.78R^2$.

n , the Stirling's approximation gives

$$\ln \frac{\langle \Gamma(C)^m \rangle^{1/m}}{\langle \Gamma(C)^n \rangle^{1/n}} \approx \ln \left(\frac{m}{n} \right) + \frac{1}{2m} \ln(2\pi m) - \frac{1}{2n} \ln(2\pi n). \quad (4)$$

We note that this estimate is independent of the loop area and the prefactors α, b in the PDFs but depends only on the moment orders m and n —and hence universal. This high order approximation shown for order 12 ($m = 12, n = 10$) in Fig. 3 agrees well with the DNS data and confirms the universal nature of the higher order normalized circulation moments. In short, the Area Rule appears to hold for the tails of the distribution, as stated in one of Migdal's papers [8].

We now examine the Area Rule for non-planar loops. Figure 4 shows a schematic of a non-planar loop C_1 which is a combination of two orthogonal squares, each of side R . The minimal surface bounded by C_1 , having zero mean curvature, is also shown. Starting from an initial guess of a surface that is discretized using triangular meshes, the gradient descent method [23, 24] is used to minimize the mean curvature and compute the triangulated minimal surface, using Mathematica[®]. Its area is approximately $1.78R^2$. If the hypothesis is right that the minimal area is what matters for the Area Rule (planar surfaces are trivially minimal surfaces), we should be able to compare $\Gamma(C_1)$ with $\Gamma(C_2)$, where C_2 is a planar loop with area = $1.78 R^2$.

To build some intuition first, we consider the asymptotic limits of $\Gamma(C_1)$ and $\Gamma(C_2)$. In the dissipative region $R/\eta \approx 1$, $\langle \Gamma(C_1)^2 \rangle^{1/2} \approx \sqrt{2}\sigma_\omega \eta^2 < 1.78\sigma_\omega \eta^2 \approx \langle \Gamma(C_2)^2 \rangle^{1/2}$, where σ_ω is the standard deviation of the vorticity. In the opposite limit $R/L \approx 1$, the PDFs approach zero for both C_1 and C_2 . For the intermediate

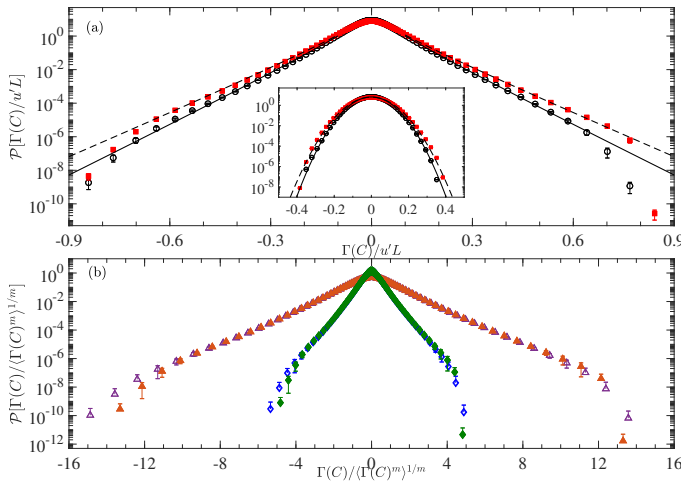


FIG. 5. Comparison of circulation PDFs for the non-planar minimal area shown in Fig. 4) and the planar loop with the same area, for $R/\eta = 150$ lying within the inertial range. (a) PDF of $\Gamma(C)/u'L$ for C_1 (open circles) and C_2 (filled squares). Straight lines are fits $\alpha \exp(-bx)/\sqrt{x}$ in $x \in [0.1, 0.7]$ with $x = |\Gamma(C)|/u'L$, $\alpha = 3.06$, $b = 22.49$ for C_1 (solid line) and $\alpha = 2.56$, $b = 19.49$ for C_2 (dashed line). The last two data points corresponding to $< 2 \times 10^{-7}\%$ samples are neglected in the fit. The inset shows the corresponding PDF for GRF with Gaussian fit $\alpha_g \exp(-bx^2)$; $\alpha_g = 6.65$, $b_g = 139.4$ for C_1 (solid line) and $\alpha = 6.36$, $b = 118.4$ for C_2 (dashed line). (b) PDF of standardized circulation $\Gamma(C)/(\Gamma(C)^m)^{1/m}$ using $m = 2$ (triangles) and $m = 8$ (diamonds) for C_1 (open symbols) and C_2 (filled symbols).

inertial range no such *a priori* knowledge is available.

Figure 5(a) compares the PDF of $\Gamma(C_1)$ and $\Gamma(C_2)$ for a fixed R in the inertial range ($= 150\eta$). The tails of the PDF (which can be fitted as before) show lower probability for C_1 than for C_2 ; hence all high-order moments of $\Gamma(C_1)$ are smaller than those of $\Gamma(C_2)$. However, the standardized PDFs shown in 5(b) for C_1 and C_2 show good agreement except possibly at the extreme tails which are prone to sampling issues, as noted already. It is noteworthy that the PDF of $\Gamma(C)/(\Gamma(C)^m)^{1/m}$ for both $m = 2$ (low order) and $m = 8$ (high order) show good collapse at the tails (except the last two data points) which indicates that even order moments of $\Gamma(C_1)$ and $\Gamma(C_2)$ match when normalized by $\langle \Gamma(C)^m \rangle^{1/m}$.

In order to examine the order dependence of the normalized PDFs in Fig. 5(a), we show the logarithm of the moments for the two loops C_1 and C_2 against the moment order in Fig. 6 in the inertial range. The moments for both loops collapse within error bars for all orders (up to $m = 12$) showing that the PDF shape is preserved for all circulation amplitudes. For the high-order moments, say 12, this quantity compares very well with the universal constant estimated by Eq. 4. Furthermore the higher order ratios approach a m^{-1} power-law dependence corresponding to GRF and is consistent with the self-similar

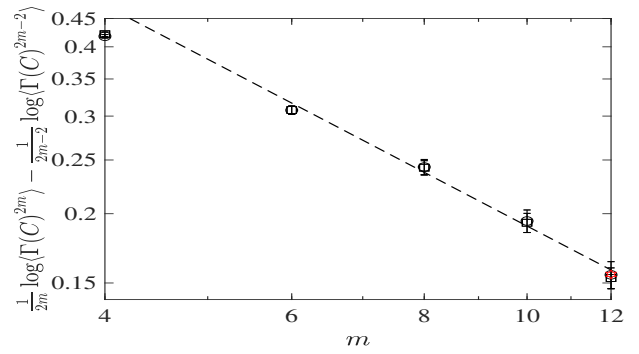


FIG. 6. Logarithm of ratio of normalized circulation moments versus moment-order m for non-planar C_1 (open circles) and planar contour C_2 (filled squares) with the same minimal area, for $R/\eta = 150$ (see Fig. 4) on log-log scales. Red hexagon at $m = 12$ corresponds to the high-order approximation from the exponential fit to the PDF (Eq. 4). Dashed line with slope -1 corresponds to the GRF slope.

nature of higher-order circulation moments [13].

Conclusions: We have examined the dependence of $\mathcal{P}(\Gamma(C))$ on the shape of the loop in both planar and non-planar cases. For the planar case, the tails of the PDFs, corresponding to large circulation amplitudes, can be fitted by $\alpha \exp(-b|\Gamma(C)|)/\sqrt{|\Gamma(C)|}$ [9, 12], which is close to an exponential, unlike for velocity differences where one needs robust stretched exponential fits [25]. The normalized high-order moments can be approximated by a universal formula, Eq. (4), that is loop-independent but order-dependent. In that sense, the Area Rule holds well for high-order moments, as theorized by Migdal [12], becoming increasingly independent of the loop geometry. For non-planar loops, the Area Rule holds only in a weak sense—i.e., only normalized PDFs collapse. This loss of generality is possibly due to non-trivial orientation of the local vorticity on the minimal surface [11]. The overall conclusion is that the tails of $\mathcal{P}(\Gamma(C))$ for loops with the same minimal area have the same form, but the scaling factor is roughly the mean square vorticity. The implication is that the average vorticity $\omega_R = \int_A \Gamma(C)/A$ attains its maximum for an inertial loop of size R when the area spanning the loop is minimal (as long as the circulation is large). The finding that large inertial vorticity is linked to the minimal area bias of turbulence could be important to fully understand the topological roots of vortex dynamics in high Reynolds number turbulence. In particular, considering that vorticity is related to the antisymmetric part of the strain rate, or to the transverse velocity increments, which is more intermittent than the symmetric part of the strain rate, or the longitudinal field [6, 7], could have an explanation in the minimal-area scaling of circulation. Elucidation of this intuition is an ongoing effort and will be reported in the future.

ACKNOWLEDGMENTS

We are grateful to A.A. Migdal for continuing and stimulating discussions and P.K. Yeung for his sustained collaboration on the DNS data. We thank A.M. Polyakov particularly for his insight on the Area Rule and E.D. Siggia for his uplifting remarks over time. This work is partially supported by the National Science Foundation (NSF), via Grant No. ACI-1640771 at the Georgia Institute of Technology. The computations were performed using supercomputing resources provided through the XSEDE consortium (which is funded by NSF) at the Texas Advanced Computing Center at the University of Texas (Austin), and the Blue Waters Project at the National Center for Supercomputing Applications at the University of Illinois (Urbana-Champaign).

* krs3@nyu.edu

- [1] A.S. Monin and A.M. Yaglom, *Statistical Fluid Mechanics: Mechanics of Turbulence*, volume II, MIT Press, 1975.
- [2] V. Yakhot and D.A. Donzis, Emergence of multiscaling in a random-force stirred fluid, *Phys. Rev. Lett.* **119**, 044501 (2017).
- [3] J. Schumacher, A. Pandey, V. Yakhot and K.R. Sreenivasan, Transition to turbulence scaling in Rayleigh-Bénard convection. *Phys. Rev. E* **98**, 033120 (2018)
- [4] U. Frisch, *Turbulence – The Legacy of A. N. Kolmogorov* (Cambridge University Press, Cambridge, UK, 1995).
- [5] K.R. Sreenivasan and R.A. Antonia, The phenomenology of small-scale turbulence. *Annu. Rev. Fluid Mech.* **29**, 435 (1997)
- [6] S. Chen, K. R. Sreenivasan, M. Nelkin and N. Cao, Refined similarity hypothesis for transverse structure functions in fluid turbulence, *Phys. Rev. Lett.* **79**, 2253–2256, 1997.
- [7] K.P. Iyer, K.R. Sreenivasan and P.K. Yeung, Scaling exponents saturate in three-dimensional isotropic turbulence, *Phys. Rev. Fluids* **5**, 054605 (2020).
- [8] A.A. Migdal, Loop equation and area law in turbulence, in *Quantum Field Theory and String Theory*, edited by L. Baulieu, V. Dotsenko, V. Kazakov, P. Windey, NATO ASI, Vol. 328 (Springer, Boston, 1995).
- [9] A.A. Migdal, Universal area law in turbulence, arXiv:1903.08613 (2019).
- [10] A.A. Migdal, Exact area law for planar loops in turbulence in two and three dimensions, arXiv:1904.05245 (2019).
- [11] A.A. Migdal, Analytic and numerical study of Navier-Stokes loop equation in turbulence, arXiv:1908.01422 (2019).
- [12] A.A. Migdal, Towards field theory of turbulence, arXiv:2005.01231 (2020).
- [13] K.P. Iyer, K.R. Sreenivasan and P.K. Yeung, Circulation in high Reynolds number isotropic turbulence is a bifractal, *Phys. Rev. X* **9**, 041006 (2019).
- [14] M. Umeki, Probability distribution of velocity circulation in three-dimensional turbulence, *J. Phys. Soc. Jpn.* **69**, 3788–3791 (1993).
- [15] K. R. Sreenivasan, A. Juneja and A. K. Suri, Scaling properties of circulation in moderate-Reynolds-number turbulent wakes, *Phys. Rev. Lett.* **75**, 433 (1995).
- [16] N. Cao, S. Chen and K.R. Sreenivasan, Properties of velocity circulation in three-dimensional turbulence, *Phys. Rev. Lett.* **76**, 616–619 (1996).
- [17] R. Benzi, L. Biferale, M. V. Struglia and R. Tripiccione, Self-scaling properties of velocity circulation in shear flows, *Phys. Rev. E* **55**, 3739 (1997).
- [18] M. Terasaki, T. Shemesh, N. Kasthuri, R.W. Klemm, R. Schalek, K.J. Hayworth, A.R. Hand, M. Yankova, G. Huber, J.W. Lichtman, T.A. Rapoport and M.M. Kozlov, Stacked endoplasmic reticulum sheets are connected by helical membrane motifs, *Cell* **154**, 285–296 (2013).
- [19] P. T. Chruściel, G.J. Galloway and D. Pollack, Mathematical general relativity: a sampler, *Bull. Amer. Math. Soc.* **47**, 567–638 (2010).
- [20] F. Bahmani, J. Christenson and P. Rangamani, Analysis of lipid flow on minimal surfaces, *Continuum Mech. Thermodyn.* **28**, 503513 (2016).
- [21] K.P. Iyer, K.R. Sreenivasan and P.K. Yeung, Reynolds number scaling of velocity increments in isotropic turbulence, *Phys. Rev. E* **95**, 021101(R) (2017).
- [22] A. Tsinober, P. Vedula and P.K. Yeung, Random Taylor hypothesis and the behavior of local and convective accelerations in isotropic turbulence, *Phys. Fluids* **13**, 1974–1984 (2001).
- [23] U. Pinkall and K. Polthier, Computing discrete minimal surfaces and their conjugates, *Exp. Math.* **2**, 15–36 (1993).
- [24] H. Schumacher (<https://mathematica.stackexchange.com/a/158356/72440>). Can mathematica solve plateaus problem (finding a minimal surface with specified boundary)? *Mathematica Stack Exchange* (2017).
- [25] P. Kailasnath, K.R. Sreenivasan and G. Stolovitzky, Probability density of velocity increments in turbulent flows, *Phys. Rev. Lett.* **68**, 2766–2769 (1992).